Lab on a Chip

Accepted Manuscript

ROYAL SOCIETY OF CHEMISTRY

www.rsc.org/loc

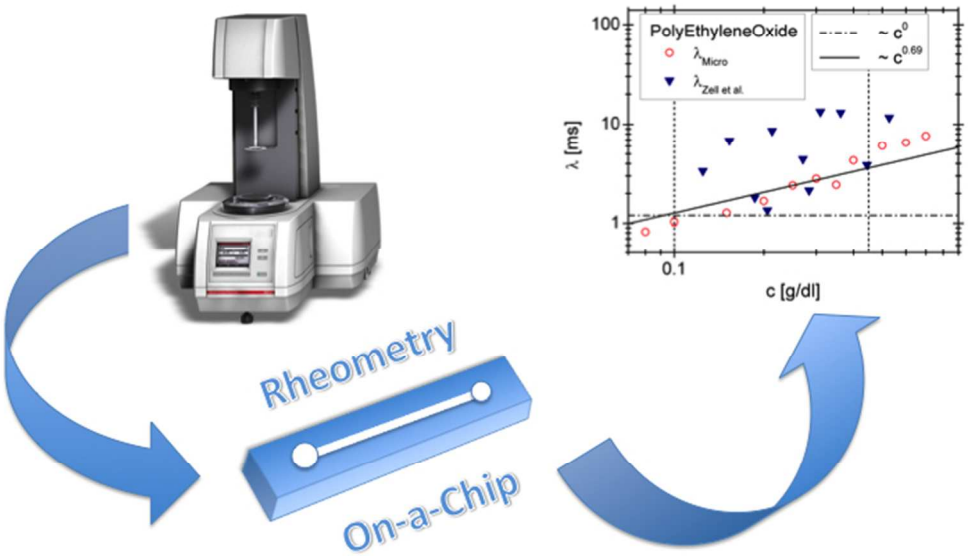

ARTICLE TYPE www. rsc.org/xxxxxx | XXXXXXXX

Rheometry-on-a-chip: measuring the relaxation time of a viscoelastic liquid through particle migration in microchannel flows

Francesco Del Giudice,*[a] Gaetano D'Avino,[b] Francesco Greco,[c] Ilaria De Santo,[a] Paolo A. Netti,[a,b] and Pier Luca Maffettone,[a,b]

Received Xth XXXXXXXXXX 20XX, Accepted Xth XXXXXXXXX 20XX
First published on the web Xth XXXXXXXXXX 200X
DOI: 10.1039/b000000x

A novel method to estimate the relaxation time of viscoelastic fluids, down to milliseconds, is here proposed. The adopted technique is based on the particle migration phenomenon occurring when the suspending viscoelastic fluid flows in microfluidic channels. The method is applied to measure the fluid relaxation times of two water-glycerol polymer solutions, in an ample range of concentrations. A remarkable improvement in the accuracy of the measure of the relaxation time is found, as compared with experimental data obtained from shear or elongational experiments available in literature. Good agreement is also found with available theoretical predictions. The proposed method is reliable, handy and does not need a calibration curve, opening an effective way to measure relaxation times of viscoelastic fluids otherwise not easily detectable by conventional techniques.

1 Introduction

Non-Newtonian fluids are widely used in our daily life[1–3]. Among them all, polymer solutions play an important role in several industrially relevant materials and applications, as in cements, paints, rubbers and, e.g., for oil recovery[4–6]. In the last few years, polymer solutions have received a growing interest in microfluidics[7–13]. Indeed, the development of techniques to control trajectories of suspended particles under continuous flow in microfluidic devices is an active research field[14], and the use of complex fluids as carrier liquids allowed the development of alternative platforms for particle manipulation, with relevant advantages over conventional techniques in terms of costs and fabrication. In this regard, it has been recently demonstrated that the addition of even small ppm of polymers in water[15] excites internal forces that promote particle migration transversely to the flow direction[7]. These migration forces are generated from the *elastic* nature of non-Newtonian fluids[7,16,17] and their entity is an increasing function of the *Deborah number* defined as $De = \lambda/t_f$, where t_f is the flow characteristic time (that depends on channel geometry and flow rate) and λ is the fluid relaxation time[9,18–21]. In real world fluids, of course, there in fact exists a spectrum of characteristic times; the λ introduced above should then be regarded as the *longest* relaxation time of the liquid, the determination of which is most useful in practice.

In a way, the fluid relaxation time can be thought of as a measure of the amount of elasticity that can be stored in the flowing sample[22]. Fluids with $\lambda \neq 0$ are defined *viscoelastic* because of their behaviour in between a viscous fluid and an elastic solid. The characteristic time λ is an important *fingerprint* of viscoelasticity, and its accurate measurement is required to properly characterize the liquid rheological properties. Exploitation of viscoelastic fluids in microfluidics, indeed, has received great attention from the scientific community[7–11] because these fluids can be used to control microparticle positions without external forces, thus implying simpler microfluidic designs[8,9,23]. An accurate knowledge of the fluid relaxation time λ is, of course, crucial in the microfluidic design[15,18]. A major problem in measuring fluid relaxation time by conventional techniques[24] arises for small values of λ (down to milliseconds). The latter is just the case, however, for polymer solutions at low polymer concentrations, which are just the ones generally used in microfluidic devices due to their capability to be pumped through small channels with acceptable pressure drops. Other important examples of fluid with quite small relaxation times are dilute solutions containing proteins, DNA or biopolymers, all of them being of interest in biological applications[15,25].

Several methods to measure the fluid relaxation time are commonly used, as reported in the literature. A first way to measure λ is through the so-called *linear viscoelastic response* experiments, in which a shearing sinusoidal deformation is applied to the material placed between parallel plates, and the viscous and elastic response of the material are sep-

[a] *Center for Advanced Biomaterials for Health Care @CRIB, Istituto Italiano di Tecnologia, P.le Tecchio 80, 80125 Naples, Italy.*
[b] *Dipartimento di Ingegneria Chimica, dei Materiali e della Produzione Industriale, Universitá di Napoli Federico II, P.le Tecchio 80, 80125 Naples, Italy. Fax: +39-081-2391800; Tel.: +39-081-7682282; E-mail: pierluca.maffettone@unina.it*
[c] *Istituto di Ricerche sulla Combustione, IRC-CNR, P.le Tecchio 80, 80125 Naples, Italy.*

arately evaluated[22]. From these measurements, it is possible to derive the fluid characteristic time by varying the oscillation frequency and observing the switch from a predominantly viscous to a predominantly elastic response[26], those responses being quantified by the loss modulus G'' and the storage modulus G', respectively. Fluids with really small relaxation times (around milliseconds), however, experience the transition from a predominantly viscous to a predominantly elastic regime at rather high frequency ($\sim$300 Hz), where the inertia of the rheometer can affect the measurement[22]. It remains possible to extrapolate the value of λ for a wide class of non-Newtonian fluids from the linear viscoelastic response data at low frequencies[22]. The fundamental bottleneck in this case resides in the possibly small values of the storage modulus G' (less than 10^{-3} Pa), which might even be not detectable by conventional rheometers[24]. In conclusion, the main difficulty of this procedure is due to technological limitations of conventional rheometers presently available on the market[27].

A second approach to determine λ is based on the measure of the *first normal stress difference* N_1 by a steady state shearing experiment[26] and on using the relation $N_1 \propto \lambda$ [22]. Because of the steady state conditions of this kind of experiment, the measure might seem easier than the one through linear oscillations[22]. However, values of N_1 are typically rather low, and are scattered,[28] and so it is difficult to extract an accurate value for λ from this method.

To overcome these difficulties, a novel method named Capillary Breakup Extensional Rheometry (CaBER) has very recently been proposed[29]. The CaBER measurement is based on the evaluation of the rheological *extensional properties* of the liquid, that are related to its viscoelasticity[30,31]. As anticipated, the main advantage of this technique is in its ability to measure relatively low values of the fluid relaxation time[8,10,29]. The intrinsic difficulties in controlling an elongational flow field should be considered, however. Moreover, Zell et al.[28] recently showed that a significant difference between the relaxation time measured by CaBER and by conventional rheometers through N_1 may exist. Specifically, it has been demonstrated that, for PolyEthylene Oxide and PolyAcrylamide solutions, λ-values taken by CaBER experiments are about forty times larger than those derived from N_1 measurements in shear[28].

It so appears that an accurate method for measuring relaxation times of an important class of non-Newtonian fluids (i.e., with low elasticity) is missing. As previously mentioned, this is a relevant issue in microfluidic applications using viscoelastic fluids, because the relaxation time is needed in the design formulas of focusing and separation devices[9–11,18,19], and an erroneous estimate would result in under/oversized devices.

Novel promising techniques for probing non-Newtonian properties have been developed just in the microfluidics field. As pointed out by Pipe and McKinley[32], the emergent field of microrheometry allows to measure rheological properties of materials, overcoming the technical limitations of conventional rheometry. Indeed, a variety of techniques to accurately measure shear and elongational viscosities have been proposed[32,33]. Very recently, Zilz et al.[24] presented a microfluidic device to derive the fluid relaxation time of low-viscoelastic polymer solutions. The idea is to relate the viscoelastic instability generated in a serpentine microchannel[34] to the fluid relaxation time λ. This technology requires a complex channel geometry (several bendings) and an efficient controlling system. The flow instability, in addition, is a delicate phenomenon, as testified by the width of the error bars in the their experimental data[24].

As mentioned above, it has been recently proven that fluid elasticity is able to efficiently focus particles along the centerline of a microfluidic channel[9–11,18,19]. In this regard, Romeo et al.[19] showed that the spatial evolution of the particle distribution along the micropipe axis is univocally determined by a single dimensionless parameter given by $\theta = De(L/D)\beta^2$, where L is the distance from the inlet, D is the channel diameter and $\beta = D_p/D$ is the confinement ratio with D_p the particle diameter. Such a scaling, valid for low Deborah numbers and for values of $\beta < 0.1$, has been validated through numerical simulations[19] and experiments[19,21]. Later, it has been shown that the same scaling holds for square-shaped microchannels as well, with the diameter D in the parameter θ replaced by the side of the channel section H[9].

So far, the scaling law with θ has been used as a design formula for a 3D focuser. Indeed, given the fluid, the flow and the geometrical properties, the required channel length to collect all the particles within a selected region around the channel centerline can be estimated. In principle, however, this procedure can be reversed: by measuring the fraction of particles migrated in a band around the centerline at a known distance from the inlet, one could extract the Deborah number and, in turn, the fluid relaxation time λ.

Motivated by these observations, we propose here a novel method to measure fluid relaxation times, as small as milliseconds. The basic idea is to obtain an indirect measurement of the fluid elasticity (hence λ) from the migration phenomenon that it causes. In this sense, the microfluidic apparatus in which particle migration occurs can be regarded as a 'microrheometer' for the suspending liquid. The technique is tested through experiments on two water-glycerol solutions of Polyethylene Oxide and on a non-ionic Polyacrylamide at several concentrations. We compare our results with those previously reported, by both pure shear and CaBER measurements[28]. Furthermore, we compare our data on those same solutions with theoretical scaling laws for λ as a function of concentration available in the literature[35,36].

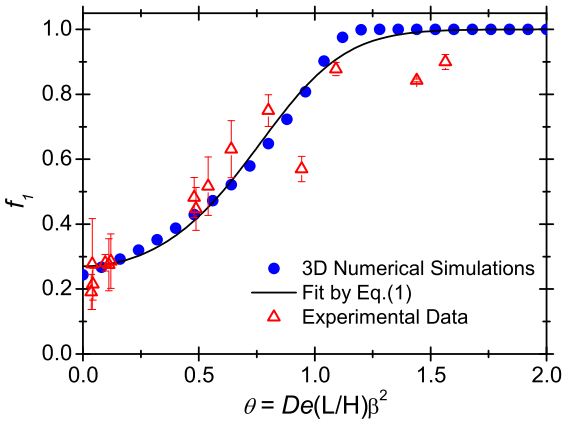

Fig. 1 Fractions of particles in the first band f_1 as a function of the dimensionless parameter $De(L/H)\beta^2$ as derived from 3D simulations (filled symbols) and experiments (open symbols) as in our previous work[9]. The black solid line is a fit of the simulation data through Eq. (1). Error bars are calculated from three sets of measurements; error bars smaller than the symbol size are not shown.

2 Working principle of the 'microrheometer'

As already mentioned in the Introduction, it has been shown[9,19,21] that viscoelastic particle migration towards the centerline of a channel is governed by a single dimensionless parameter $\theta = De(L/H)\beta^2$. In Figure 1, we report the data taken from our previous work[9] (open symbols) along with numerical predictions (blue closed circles) obtained through a (dimensionless) migration velocity of the form $V_M(r) \propto -De\,\beta^2\,r$, with r the distance of the particle from the channel centerline. In this figure, f_1 is the fraction of particles within a circular region in the channel cross-section around the centerline, with radius approximately equal to a particle diameter. (For a clearer definition of this innermost band around the centerline, see Figure 3(b) below.) The experiments of Del Giudice et al.[9] were carried out by using a water-polymer solution of PolyVinylPyrrolidone (PVP) at 8% wt. This fluid has a constant viscosity but a non-zero viscoelasticity[7–9,19]. Numerical simulations[9,19] were performed at low Deborah numbers (thus non-linear effects such as shear-thinning are not accounted for), and for relatively low confinement ratios ($\beta < 0.15$). The good agreement between experiments and simulations confirmed the validity of the above mentioned scaling[9].

Notice that the trend shown in Figure 1 is, in principle, valid for any viscoelastic fluid, provided that the Deborah number is low, which holds for most of viscoelastic fluids with λ of the order of milliseconds. In other words, within the assumptions discussed above, the blue symbols in Figure 1 represent an *universal mastercurve* describing the spatial evolution of the fraction of particles in the inner band f_1 along the channel axis. Thus, no calibration curve is needed as the experimental conditions, such as channel and particle dimensions, are varied. Therefore, for a given set of geometrical parameters (cross-section channel side length H, confinement ratio β) and flow rate Q, by measuring the fraction of particles f_1 at a distance L from the inlet, the relaxation time λ (included in De) can be evaluated from the mastercurve.

The previous arguments are based on the predominance of purely elastic effects, with the neglecting of other hydrodynamic phenomena[19]. As a matter of fact, particles subjected to flow in a microfluidic straight channel, even in the case of a Newtonian suspending liquid, can experience hydrodynamic effects due to inertia, such as the Segré-Silberberg[37] effect and the Saffman lift force[38]. It is readily shown, however, that both these inertia-driven migration effects are negligible with respect to the viscoelastic migration. Indeed, the ratio between the Segré-Silberberg and viscoelastic migration velocity can be estimated as proportional to $(Re_f/De)\,\beta$[18,39], with Re_f the Reynolds number of the fluid. Similarly, the ratio between the Saffman[38] and viscoelastic migration velocity can be estimated as proportional to $\sqrt{Re_p}V_s/(De\beta^2)$ with Re_p the Reynolds number of the particle and V_s the so-called 'slip velocity' i.e., the longitudinal actual velocity of the particle minus the fluid velocity at the same position. Thus, it is apparent that, when both these two velocity ratios are less than unity, the only relevant mechanism of migration is the one due to viscoelasticity. As shown below, our experiments are so designed as to meet the just mentioned working conditions; hence, since all the hydrodynamic effects are negligible, the measured λ corresponds to the elastic relaxation time only.

As a further confirmation that the characteristic time measured in our experiments is the constitutive relaxation time of the suspending fluid, we compare such constitutive time with the only other characteristic time present in our situation, namely, the so-called 'particle hydrodynamic characteristic time' given by $\tau = \rho_d d^2/(18\eta)$[40]. It is readily shown that the ratio τ/λ comes out proportional to $(Re_p/De)\,\beta$ which, in our conditions, is much smaller than unity.

The blue filled symbols in Figure 1 were derived from 3D numerical simulations[9], thus no analytical curve is available. It is helpful to adopt an interpolating analytical expression through the simulation data in Figure 1 in order to easily obtain the θ-value from the measured f_1. We find that the following function describes the data with a sufficient accuracy:

$$f_1 = \frac{1}{1 + Be^{-C\theta^2}} \qquad (1)$$

(Equation (1) has to be regarded as a simple formula describing the calculated data, with no physical justification.) This equation is reported with the black line in Figure 1, with $B = 2.7$ and $C = 2.75$ obtained by fitting the simulation data.

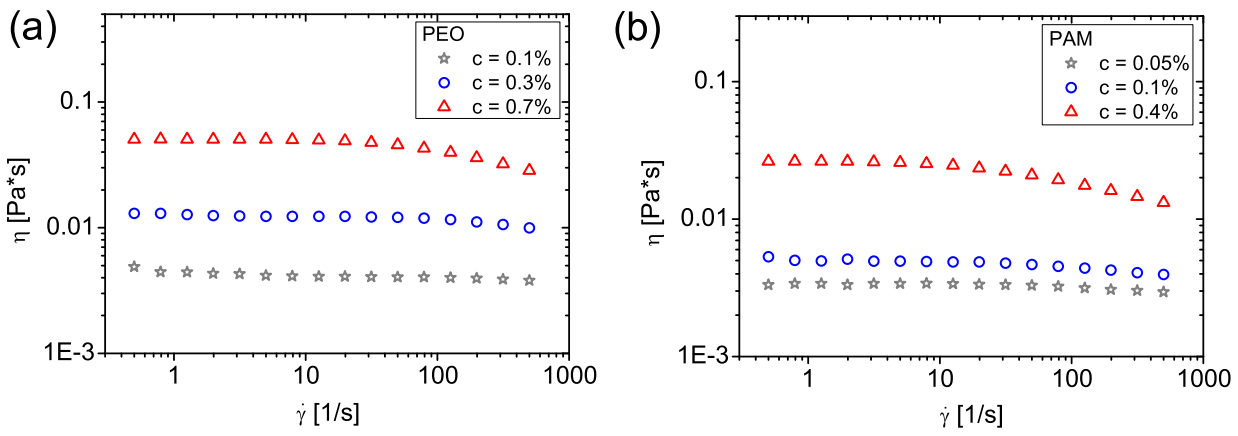

Fig. 2 (a) Steady shear viscosity η for the aqueous PEO solutions at three different concentrations as a function of the shear rate $\dot{\gamma}$. (b) Steady shear viscosity η for the aqueous PAM solutions at three different concentrations as a function of the shear rate $\dot{\gamma}$.

The solid line well fits the data except around the bending towards the plateau. As discussed below, measurements should be avoided in this region, thus the deviations from Eq. (1) are not relevant for our purposes.

By inverting the equation above, we get:

$$\theta = \sqrt{\frac{1}{C}\ln\left(\frac{f_1 B}{1-f_1}\right)} \qquad (2)$$

that allows to directly compute θ from f_1. The procedure to evaluate the normalised particle fraction f_1 is decribed in the next section.

A final remark about the choice of the θ-value is in order. The trend reported in Figure 1 reaches a plateau at $\theta > 1$, i.e. all the particles have been focused in the circular band around the channel centerline. In this case, the mastercurve is not invertible. Thus, a feasible measure of the fluid relaxation time through f_1 requires $\theta < 1$. From the definition of θ, it so appears that such a parameter can be changed in several ways. However, the channel side length H needs to be selected sufficiently low in order to guarantee negligible inertial effects. The confinement ratio must satisfy the condition $\beta < 0.15$ but, at the same time, the particle size should be sufficiently large to avoid diffusion, and problems in particle tracking experiments. Recommended ranges for these two parameters are $H = 50 - 100$ μm with $\beta = 0.05 - 0.1$. Therefore, those two quantities are constrained within quite small intervals. On the other hand, the flow rate Q and the distance from the channel inlet L can be easily adjusted in order to get the θ value in the correct range. More specifically, to speed-up the measurement, it is desirable to use relatively high flow rates, with the only limitation due to avoiding the arising of inertial effects that can alter the phenomenon. In conclusion, the distance from the inlet of the observation section, proportional to θ, is the tunable parameter to perform reliable measurements.

3 Materials and methods

3.1 Suspending fluids and particles

The solvent used in this work is a glycerol-water solution at 25% wt of glycerol, in order to avoid sedimentation problems. The solvent viscosity is $\eta = 0.002$ Pa·s. Two viscoelastic fluids are considered: a PolyEthylene Oxide (PEO) with average molecular weight $M_w = 4$ MDa (Sigma-Aldrich) and at several mass concentrations ranging from 0.08 g/dl to 0.8 g/dl wt in glycerol-water mixture and a non-ionic PolyAcrylamide (PAM) with average molecular weight $M_w = 5 - 6$ MDa at several mass concentrations ranging from 0.05 g/dl ppm to 0.8 g/dl wt in glycerol-water mixture.

Rheological measurements are carried out to derive the zero-shear viscosity of the polymer solutions. In this way, we can compare the λ-values measured by the proposed method with those provided from the available theoretical scaling laws[36]. The fluid rheological properties are measured by a stress-controlled rheometer (Anton Paar MCR 302 rheometer), with cone and plate geometry with diameters of 60 mm and with a solvent-trap to avoid fluid evaporation.

Figure 2(a) shows the measured shear viscosity η for the aqueous PEO solutions at three different concentrations. When $c = 0.1\%$ and $c = 0.3\%$, PEO solutions behave like a constant-viscosity fluid, whereas at $c = 0.7\%$ (the highest value of concentration used in our work) it starts to show a weak shear-thinning behaviour from $\dot{\gamma} \sim 100\ s^{-1}$. The shear rheology for PAM solutions is showed in Figure 2(b). The shear thinning region here starts earlier, from $\dot{\gamma} \sim 30\ s^{-1}$. We

remark that all our experiments are carried out in the zero-shear region, far away from the shear thinning zone for both fluids.

Polystyrene (PS) particles (Polysciences) with diameter $D_p = 10$ μm and density $\rho_p = 1.05$ g/l are used. A dilute suspension with a volume fraction $\phi = 0.01\%$ is prepared. Particles are added to the matrix that is put first in a mixer (Vortex, Falc Instruments) to guarantee a good dispersion and then in an ultrasonic bath (Falc Instruments) to remove air bubbles. This procedure is repeated before each experiment.

3.2 Microfluidic device

The microrheometer consists in a simple square-shaped cross-section channel made of polymethylmethacrylate (PMMA, substrate thickness 1 mm, Goodfellow). The channel is milled on the PMMA substrate using a micromilling machine (Minitech CNC Mini-Mill) following the procedure reported in our previous works[9]. After fabrication, the channel is bonded on another PMMA substrate by immersing the two pieces in absolute ethanol (from Sigma-Aldrich) for about 20 minutes, clamping them together, and putting the device in the oven at $T = 40^\circ$ C for about two hours.

A schematic picture of the channel geometry is reported in Figure 3(a). The entrance (triangular shape from the top view, left side of Figure 3(a)) is designed in such a way to assure a smooth velocity field from the inlet to the main channel[9]. The relevant dimensions of the device are shown in the figure. The dimension of the cross-section side is $H = 100$ μm giving a confinement ratio $\beta = D_p/H = 0.1$. The total length of the channel is $L_{tot} = 9$ cm. An image of the real device is shown in Figure 3(c).

The flow rate is controlled by a syringe pump (Nemesys) with glass syringes. We wait for 20 minutes before each measurement in order to reach steady-state conditions. The range of flow rates used in our experiments is from 0.5 μl/min to 8 μl/min.

With data as reported in the present and the previous sections, we can now evaluate the quantities $(Re_f/De)\beta$ and $\sqrt{Re_p}V_s/(De\beta^2)$ that, as discussed in section 2, gauge inertial effects (Segré-Silberberg and Saffman lifts, respectively) with respect to the viscoelastic ones. In the worst situation, i.e., at the highest flow rate and for the lowest viscosity liquid, inertial lifts turn out to be at least two order of magnitudes lower than the viscoelastic lift. We can therefore confirm that, since all the hydrodynamic effects are negligible, the characteristic time measured in our experiments corresponds to the constitutive relaxation time of the suspending liquid.

3.3 Particle distribution measurements

Particles flowing in the channel are observed using a straight microscope (Olympus BX-73) with a 4x objective to reach the best depth of field without losing information on particle motion. Image sequences are collected with a fast camera (IGV-B0620M, Imperx) at a frame rate variable between 30 and 400 fps depending on the flow rate. The observations are made at a fixed distance of $L = 8$ cm from channel inlet (see Figure 3(d) for a sample image of the alignment experiment). For all the fluids considered in this work, such a distance assures that the θ-value is lower than 1. All the experiments are performed at room temperature.

Following our previous work[9], we divide the channel cross-section in six bands as reported in Figure 3(b). The bands are progressively numbered for increasing distances from the centerline, so $k = 1$ denotes the innermost band (see Figure 3b). The boundaries of each band are equispaced along the $x-$axis (see Figure 3b) and denote the contours of the translational velocity of the particles along the flow direction, calculated by numerical simulations.[9]. Notice that this choice is arbitrary. However, the adopted division has been proven to give reliable and reproducible measurements, provided that at least one hundred of particles are counted.[9] We perform particle tracking experiments in order to derive the normalized fraction of particles in the first band f_1. As described elsewhere[9], we adopt the following formula to compute f_1:

$$f_1 = \frac{\frac{n_1}{A_1\overline{v}_1}}{\sum_{k=1}^{6}\frac{n_k}{A_k\overline{v}_k}} \tag{3}$$

where n_k is the number of particles flowing in the band k, A_k is the cross-sectional area of the $k-$th band and $\overline{v}_k$ is the average velocity of the fluid enclosed in the $k-$th band. The normalization through the product $A_k\overline{v}_k$ in Eq. (3) is made to properly take into account that different bands have different areas and velocities.

Of course, the values of A_k and $\overline{v}_k$ depend on the selection of the bands. We report in Table 1 the areas A_k, the average velocities $\overline{v}_k$ for each band, as well as the isovelocity values corresponding to the boundaries between the bands normalized by the maximum particle velocity (on the channel centerline). The evaluation of the number of particles n_k can be, then, readily performed by comparing the translational velocities of the particles measured through particle tracking experiments with the values reported in this Table. In conclusion, the data supplied in Table 1 are all the information needed to evaluate f_1 from Eq. (3); the θ-value can be, then, readily calculated from Eq. (2), providing the measurement of the fluid relaxation time.

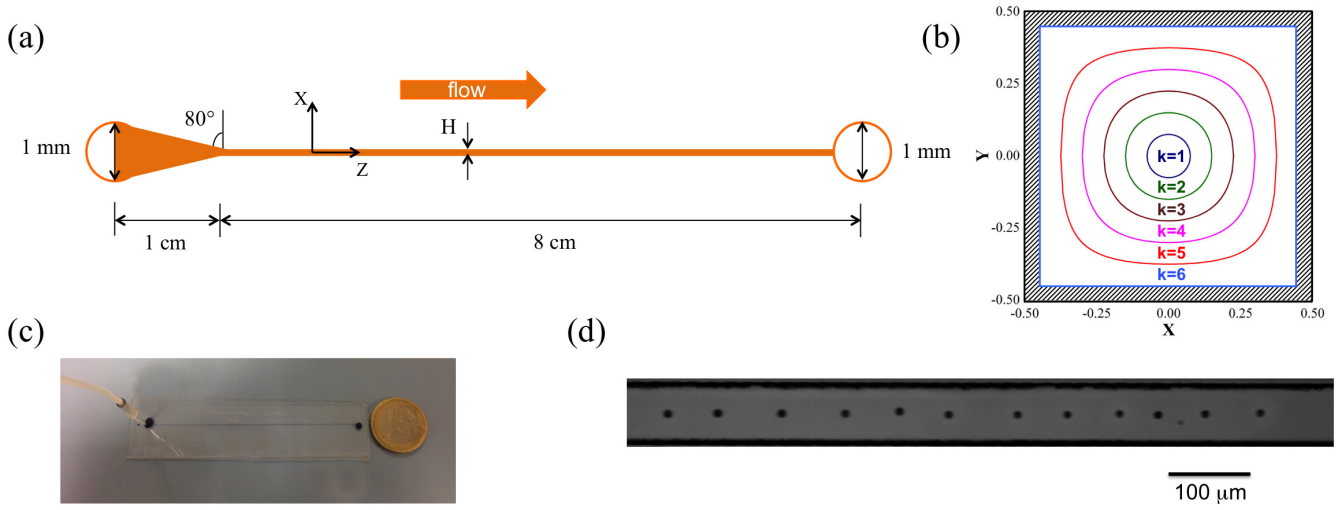

Fig. 3 (a) Schematic representation of the channel used in the experiments, $H = 100\ \mu$m. A smooth entrance at the channel ends are fabricated in order to guarantee an uniform particle distributions. In the figure, the relevant dimensions are reported. The dimensions along X and Z are not in scale. (b) Concentric bands dividing the channel cross-section used to compute the particle distributions. X and Y are the dimensionless coordinates of the channel cross-section. The shaded regions denote zones of the cross-section unaccessible to the particles. The bands are progressively numbered from the inner one ($k = 1$) to the outer one ($k = 6$). Notice that the first band has almost the same dimension of the particle. (c) Image of the 'microrheometer' device used in this work. (d) Snapshot of particle alignment at 8 cm from the inlet.

Band	$V_{k,k+1}/V_{max}$	A_k	$\bar{v}_k$
1	0.98	0.018	0.99
2	0.92	0.054	0.95
3	0.82	0.093	0.87
4	0.67	0.138	0.75
5	0.46	0.192	0.57
6	-	0.507	0.18

Table 1 For each band (first column) we report: values of the isovelocities $V_{k,k+1}$ common to the bands k and $k+1$ (see Figure 3(b)) normalized by the maximum velocity V_{max} (second column); the areas A_k (third column); the average fluid velocities $\bar{v}_k$ (fourth column).

4 Experimental results and discussion

4.1 General background

The rheological behaviour of polymer solutions is strongly dependent on concentration and on the nature of the solvent[22,36]. It has been theoretically predicted and experimentally demonstrated that the physico-chemical and rheological behaviour of a solution with flexible polymers drastically changes at some characteristic concentrations[35,36]; of interest here are the overlap concentration c^* and the entanglement concentration c_e. Such two quantities mark the transitions between different concentration regimes, from dilute to semidilute unentangled (through c^*) and to semidilute entangled (through c_e), by increasing polymer concentration.

Different scaling laws apply depending on the polymer solution's concentration regime[36]. These laws also contain important information about the 'quality' of the solvent for the dissolved polymer[29,35,36] through the *fractal polymer dimension* ν, that somehow quantifies the volume pervaded by a polymer coil within the liquid. A value of $\nu = 0.5$ identifies the so called *θ-solvent*, while $\nu = 0.6$ defines a *good solvent*[41].

In this work, dealing with rheological characterisation, we are specifically focused on the scaling laws for the zero-shear viscosity[22]. As a matter of fact, we will mainly use in the following a nondimensional viscosity η_{sp} (specific viscosity), defined as:

$$\eta_{sp} = \frac{\eta}{\eta_s} - 1 \tag{4}$$

where η is the viscosity of the polymer solution and η_s is the solvent viscosity. The scaling law for η_{sp} as a function of concentration and fractal polymer dimension ν for Dilute, SemiDilute Unentangled and SemiDilute Entangled regime are respectively[35,36]:

$$\eta_{sp,D} \propto c \qquad \eta_{sp,SDU} \propto c^{1/(3\nu-1)} \qquad \eta_{sp,SDE} \propto c^{3/(3\nu-1)} \tag{5}$$

with obvious meaning of the subscripts.

Specific viscosities will be used to characterise different concentration regimes for the two polymer solutions invstigated here. However, since our main purpose is to perform measurements of the relaxation time (through migration effects, as described above), we also need to report the predicted scaling laws for the relaxation time, which are:

$$\lambda_D \propto c^0 \qquad \lambda_{SDU} \propto c^{(2-3\nu)/(3\nu-1)} \qquad \lambda_{SDE} \propto c^{3(1-\nu)/(3\nu-1)} \tag{6}$$

for the dilute, semidilute unentangled and semidilute entangled regime, respectively[35,36].

Regarding the polymer solutions used in this work, values for the ν coefficient are available from the literature. Tirtaatmadja et al.[29] took several experiments on PEO solutions, at different molecular weight, in water and glycerol-water mixtures, finding $\nu = 0.55$ in all cases, in good agreeement with the Polymer Handbook[42] and with other works[43,44]. Regarding PAM solutions, it is well known that strongly different behaviours can show up, depending on the synthesis procedure, leading to the nomenclature of *ionic* and *non-ionic* PAM[45–48]. In particular, non-ionic PAM, as the one used in our rheological experiments, behaves like a neutral flexible polymer. Some authors[49] characterise several ionic high molecular weight PAM (hmwPAM) solutions in water and glycerol-water mixtures, finding that water and glycerol-water mixtures up to 50% wt are good solvents. It has also been found that, for non-ionic hmwPAM solutions, water is a good solvent with $\nu = 0.585$[50]. To the best of our knowledge, no ν data are available for non-ionic hmwPAM in glycerol-water mixtures, as the ones we use. On the basis of the just mentioned results, however, we adopt a value $\nu = 0.585$ in our case.

4.2 Fluids rheology

With those values of ν as stated above, we take several rheological experiments in order to characterise the different concentration regimes for our polymer solutions, and compare our results with the theoretical predictions[35,36]. Figure 4(a-b) shows the specific viscosities of PEO 4 MDa and PAM 5-6 MDa, respectively, as a function of concentration. Let us discuss the PEO solutions first.

Dashed line and solid line are the theoretical predictions of the specific viscosity for a neutral polymer in good solvent, with $\nu = 0.55$. Dashed line refers to the dilute regime while solid one refers to the semidilute unentangled regime. With $\nu = 0.55$, the expressions for η_{sp} in those regimes are (from Eq. (5)):

$$\eta_{sp,D} \propto c \qquad \eta_{sp,SDU} \propto c^{1.36} \tag{7}$$

The curves given by Eq. (7) can of course be vertically shifted depending on prefactors, which however are not easily assessed from theoretical arguments. Thus, in order to properly identify the different regimes, i.e. the vertical positions of the two curves, we proceed as follows. We fit different subsets of our complete data set with the available prediction of Eq. (7); we then choose the data subset with the highest number of data points that gives the coefficient of determination R^2 closest to the unity as the subset representative of a concentration regime. For example, we take the data subset ranging from 0.08 g/dl $< c <$ 0.8 g/dl and evaluate the R^2 imposing the equation $\eta_{sp,SDU} = A\,c^{1.36}$. We thereafter compare this R^2 value with the one obtained by choosing a narrower data subset, e.g. in the range 0.1 g/dl $< c <$ 0.6 g/dl, and choose the subset with the R^2 value closer to unity. By repeating this procedure, we arrive to the curves reported in Figure 4(a), thus identifying the dilute and semidilute unentangled regime. From Figure 4(a) it is now possible to estimate the value of the overlap concentration c^*, and also that of the entanglement concentration c_e: we find $c^*_{\mathrm{PEO}} \sim 0.1$ g/dl and $c_{\mathrm{e,PEO}} \sim 0.45$ g/dl. Indeed, when $c > 0.45$ g/dl, experimental data clearly start to deviate from the theoretical prediction for the semidilute unentangled regime, suggesting the transition to a new regime.

Figure 4(b) shows the specific viscosity η_{sp} of PAM solutions, as a function of the concentration. The theoretical predictions are here obtained by assuming $\nu = 0.585$ in Eq. (5):

$$\eta_{sp,D} \propto c \qquad \eta_{sp,SDU} \propto c^{1.32} \tag{8}$$

Also in this case, by following the same procedure previousy described, we determine the prefactors in Eq. (8) and then draw the dashed and the solid lines in Figure4(b). We estimate an overlapping concentration $c^*_{\mathrm{PAM}} \sim 0.1$ g/dl and an entanglement concentration $c_{\mathrm{e,PAM}} \sim 0.35$ g/dl.

We alert the reader that the obtained values for the transition concentrations for both the examine polymer solutions are, in fact, only indicative values, as transitions between different regimes are, of course, never sharp. We however surmise that our estimate for the *width* of the semidilute unentangled regime is a conservative one.

We can compare the just obtained c^* values with the ones directly obtained by looking at the plot of the reduced viscosity $\eta_{red} = \eta_{sp}/c$ as a function of concentration, following a well known procedure[22]. Figure 4(c) shows such plots for PEO 4 MDa solutions (upper graph) and for PAM 5-6 MDa solutions (lower graph), respectively. Notice that this procedure is carried out in the dilute and semidilute unentangled regimes. For the PEO solutions, the intercept of the red curve for $c \to 0$ gives the intrinsic viscosity $[\eta]_{\mathrm{PEO}} = 8$ dl/g, from which $c^*_{\mathrm{PEO}} = 1/[\eta]_{\mathrm{PEO}} = 0.12$ g/dl (Flory theory[29]) and $c^*_{\mathrm{PEO}} =$

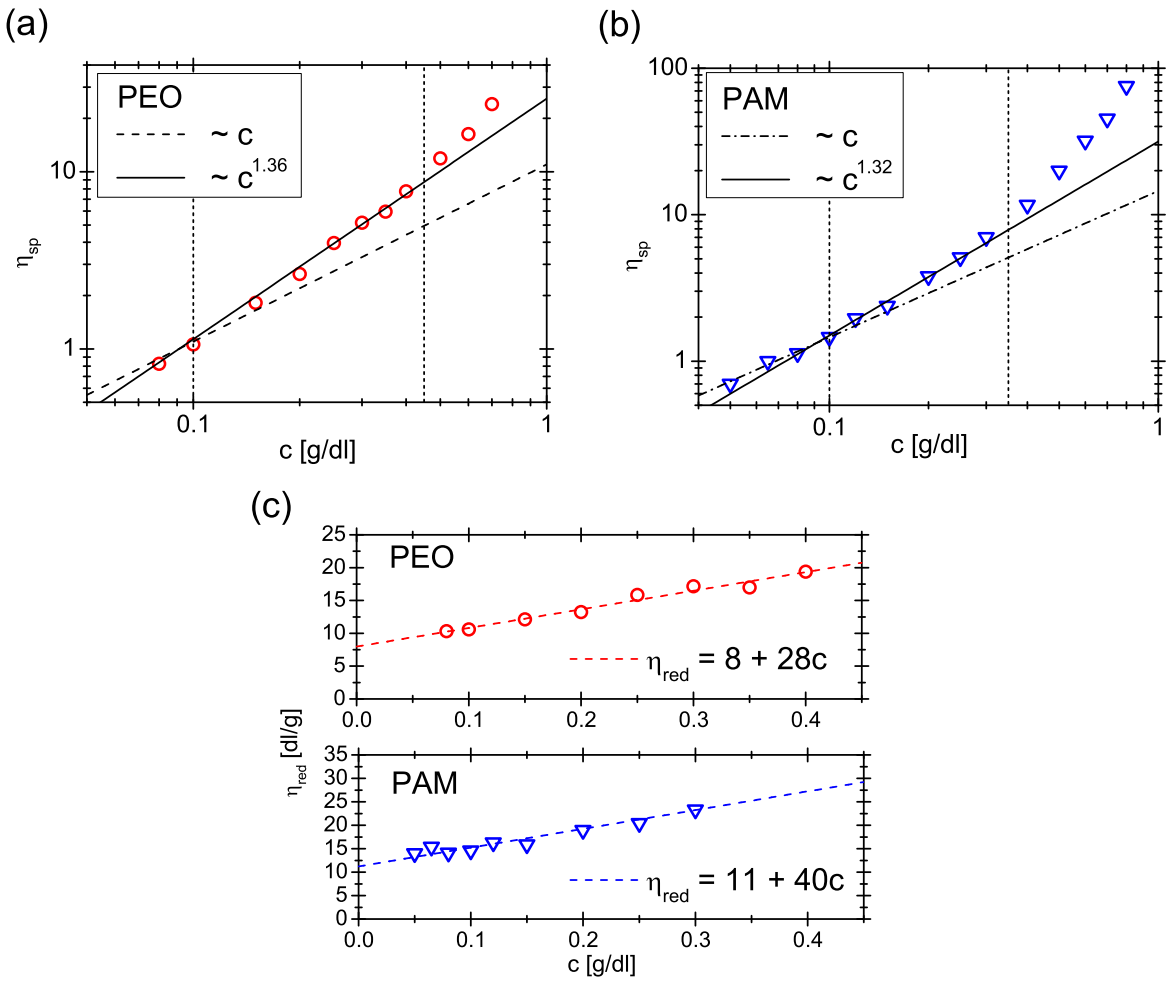

Fig. 4 Rheological characterization of PEO and PAM. (a) Plot of the specific viscosity as a function of concentration for PEO 4 MDa. Dashed and solid lines are the scaling law predictions for a neutral polymer with fractal dimension $\nu = 0.55$ in the dilute and semidilute unentangled regime, respectively. Error bars, estimated from the average of the zero-shear viscosity values in the rheology curves, are always smaller than the symbol size. Vertical black dashed lines are an estimate of the values of c^* (left) and c_e (right), respectively (see text). (b) Plot of the specific viscosity as a function of concentration for PAM 5-6 MDa. Dashed and solid lines are the scaling law predictions for a neutral polymer with fractal dimension $\nu = 0.585$ in the dilute and semidilute unentangled regime, respectively. Error bars, estimated from the average of the zero-shear viscosity values in the rheology curves, are always smaller than the symbol size. Vertical black dashed lines are an estimate of the values of c^* (left) and c_e (right), respectively. (c) Plot of the reduced viscosity η_{red} for the PEO 4 MDa (upper graph) and PAM 5-6 MDa (lower graph), as a function of the concentration c in the dilute and semidilute unentangled regimes. The intercept of the two lines for $c \to 0$ is the *intrinsic viscosity* $[\eta]$.

$0.77/[\eta]_{\mathrm{PEO}} = 0.096$ g/dl (Graessley theory[51]), both in good agreement with the value $c^*_{\mathrm{PEO}} \sim 0.1$ g/dl estimated above. For the PAM solution, the intercept of the blue curve gives $[\eta]_{\mathrm{PAM}} = 11$ dl/g, from which it is $c^*_{\mathrm{PAM}} = 1/[\eta]_{\mathrm{PAM}} = 0.068$ g/dl (Flory) and $c^*_{\mathrm{PAM}} = 0.77/[\eta]_{\mathrm{PAM}} = 0.09$ g/dl (Graessley), again in good agreement with $c^*_{\mathrm{PAM}} \sim 0.1$ g/dl.

4.3 Determination of the fluids relaxation times

With the characterisation of both polymer solutions completed, i.e., having identified their respective concentration regimes, we proceed now to show the predictions for the relaxation time, and to compare our data and those by Zell et al.[28] with such predictions. Let us start to discuss the PEO solutions first. The following expressions should hold (see Eq. (6) with $\nu = 0.55$):

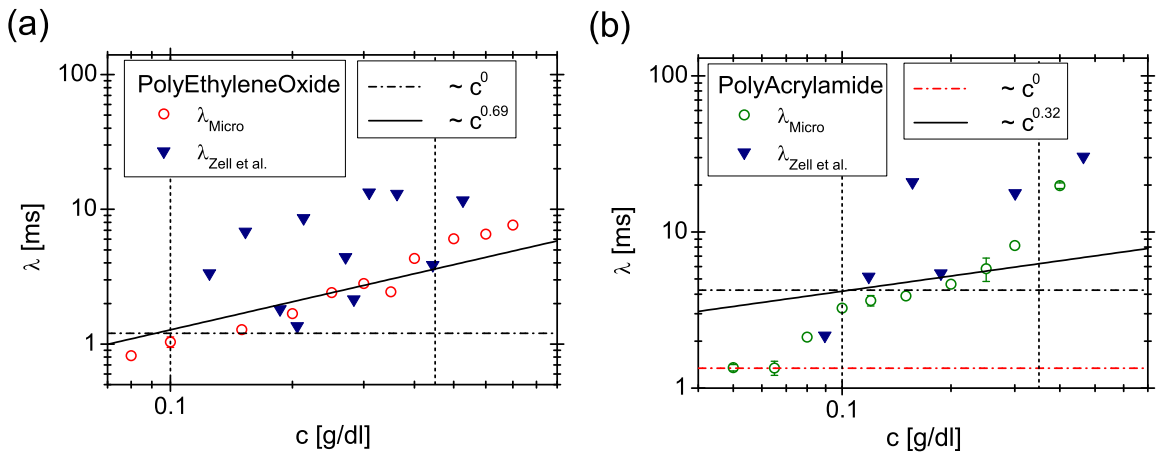

Fig. 5 (a) Comparison between experimental results on the fluid relaxation time λ derived from our 'microrheometer' with the ones by Zell et al.[28], for PEO 4 MDa at different concentrations. Dashed line is the Zimm prediction for the dilute regime, solid line is the Rouse prediction for the semi-dilute unentangled regime, both of then with $\nu = 0.55$. Vertical black dashed lines are at c^* (left) and c_e (right), respectively. Error bars, evaluated by dividing the statistical samples in three sets and calculating the standard deviation between the three λ-values, are smaller than the symbol size. (b) Comparison between experimental results on the fluid relaxation time λ derived from our 'microrheometer' with the ones by Zell et al., for PAM 5-6 MDa at different concentrations. Dashed lines are two possible Zimm predictions for the dilute regime. Solid line is the Rouse prediction for the semi-dilute unentangled regime. All these lines are for $\nu = 0.585$. Black dashed line is the expected theoretical prediction below c^*_{PAM}. Red dashed line is the Zimm prediction through our own data for $c << c^*_{\mathrm{PAM}}$. Vertical black dashed lines are at c^*(left) and c_e(right), respectively. Error bars are evaluated by dividing the statistical samples in three sets and calculating the standard deviation between the three λ-values. Error bars smaller than the symbol size are not shown.

$$c < c^*_{\mathrm{PEO}} \sim 0.1 \text{ g/dl} \qquad \lambda \propto c^0 \tag{9}$$

$$c^*_{\mathrm{PEO}} < c < c_{\mathrm{e,PEO}} \sim 0.45 \text{ g/dl} \qquad \lambda \propto c^{0.69} \tag{10}$$

Figure 5(a) shows the relaxation time λ as a function of the concentration. Vertical dashed lines are the estimate of the overlap concentration c^*_{PEO}(left) and of the entanglement concentration $c_{\mathrm{e,PEO}}$(right) from our previous analysis. It is apparent from Figure 5(a) that most of our λ data(red circles) are in the semidilute unentangled regime. We draw the black line in Figure 5(a), i.e. the theoretical prediction as in Eq. (10), after having computed the prefactor from the data subset in between the two vertical dashed lines. Notice how our data are less scattered with respect to the those by Zell et al.[28], obtained from steady shear measurements of N_1. Our experimental data are also in rather good agreement with the power-law prediction of Eq. (10). In particular, by applying the fitting procedure described above for data in the semidilute unentangled regime we find $R^2_{\mathrm{PEO,micro}} = 0.96$, whereas it is $R^2_{\mathrm{PEO,Zell\ et\ al.}} = 0.49$ for Zell et al. data[28]. Hence, our results are largely less scattered than those obtained from standard rheometrical measurements.

Figure 5(b) shows the relaxation time λ as a function of the concentration for the PAM solutions. The scaling law are here obtained by assuming $\nu = 0.585$ in eq. (6):

$$c < c^*_{\mathrm{PAM}} \sim 0.1 \text{ g/dl} \qquad \lambda \propto c^0 \tag{11}$$

$$c^*_{\mathrm{PAM}} < c < c_{\mathrm{e,PAM}} \sim 0.35 \text{ g/dl} \qquad \lambda \propto c^{0.32} \tag{12}$$

Most of the data are again in the semidilute unentangled regime, and show again a good agreement with the power-law of Eq. (12) (the prefactor was obtained again from data in between c^*_{PAM} and $c_{\mathrm{e,PAM}}$ only), with $R^2_{\mathrm{PAM,micro}} = 0.96$. Notice that, also in this case, the R^2 calculated from the rheometrical data by Zell at al.[28] ($R^2_{\mathrm{PAM,Zell\ et\ al.}} = 0.45$) is much smaller than our own, thus confirming that conventional rheometrical techniques are less effective than the microrheometrical technique proposed here. For $c < c^*_{\mathrm{PAM}}$, conversely, data are not in strict agreement with theoretical predictions. Indeed, data would be expected to lye on the black horizontal dashed line of Figure 5(b), whereas they tend to lye(for $c \ll c^*_{\mathrm{PAM}}$) on the red dashed line of the same plot. This behaviour possibly evidentiates that the dilute-semidilute unentangled transition is not sharp. The same kind of discrepancy with the theory around c^* had been previously found by Tirtaatmadja et al.[29] on PEO solutions. Indeed they found that, for $0.05\ c^* < c < c^*$, the relaxation time $\lambda \propto c^{0.65}$, in contrast with the Zimm prevision in Eq. (6); they also found that the Zimm prevision is only recovered when $c \ll c^*$. This unexplained behaviour is, in fact, similar to our observations below c^*_{PAM}. However, more data

in the low concentration range would be needed to confirm or deny the presence of such pre-transitional behaviour.

5 Conclusions

In this work, we present a novel method to measure the relaxation time λ of viscoelastic fluids down to milliseconds. The idea is to exploit the relation between the characteristic time λ and the phenomenon of viscoelasticity-induced particle migration in microchannel flow[7–10,18]. We demonstrate that an accurate measurement of λ can be obtained from the measurements of the normalised particle fraction f_1 at the axis of the microchannel. We point out that the measurements of f_1 does require rather standard particle tracking experiments, thus making the proposed method handy and relatively easy to be performed.

The performances of the 'microrheometer' are tested on two glycerol-water solutions on PEO and PAM solutions at various concentrations. The obtained data are reliable, accurate, and in good agreement with theoretical predictions[35,36].

The range of applicability of our novel technique is comparable with that recently proposed by Zilz et al.[24]. Our device, however, is by far simpler in terms of design and working principles. Indeed, the working principle of our 'microrheometer', being based on the 'universal' curve in Figure 1, does not need a calibration procedure. In this regard, we remark that the measurements performed in this paper exploit a square-shaped microchannel with side $H = 100\,\mu$m. We recall that, for a fixed confinement ratio β, the parameter θ (the abscissa in Figure 1) scales as $1/H^4$. Hence, very low Deborah numbers might be investigated by using smaller channel side lengths[9], with a remarkable increase in the sensitivity of the 'microrheometer', i.e., in the ability to measure very low relaxation times.

References

1 R. P. Chhabra and J. F. Richardson, *Non-Newtonian flow and applied rheology: engineering applications*, Butterworth-Heinemann, 2011.

2 A. Dickie and J. Kokini, *J Food Sci*, 1983, **48**, 57–61.

3 J. Binshtock, R. S. Cabanas and R. Catiis, *Continuous process for making a non-Newtonian paste or cream like material*, 1993, US Patent 5,236,696.

4 D. Jones and K. Walters, *Rheol Acta*, 1989, **28**, 482–498.

5 T. Oishi and J. M. Prausnitz, *Ind Eng Chem*, 1978, **17**, 333–339.

6 R. Pasquino, F. Nicodemi, V. Vanzanella, R. Alfani and N. Grizzuti, *Rheol Acta*, 2013, **52**, 395–401.

7 A. Leshansky, A. Bransky, N. Korin and U. Dinnar, *Phys Rev Lett*, 2007, **98**, 234501.

8 S. Yang, J. Y. Kim, S. J. Lee, S. S. Lee and J. M. Kim, *Lab Chip*, 2011, **11**, 266–273.

9 F. Del Giudice, G. Romeo, G. D'Avino, F. Greco, P. A. Netti and P. L. Maffettone, *Lab Chip*, 2013, **13**, 4263–4271.

10 H. Lim, J. Nam and S. Shin, *Microfluid Nanofluid*, 2014, 1–10.

11 J. Nam, H. Lim, D. Kim, H. Jung and S. Shin, *Lab Chip*, 2012, **12**, 1347–1354.

12 P. Tabeling, *Introduction to microfluidics*, Oxford University Press, 2010.

13 G. M. Whitesides, *Nature*, 2006, **442**, 368–373.

14 A. Lenshof and T. Laurell, *Chem Soc Rev*, 2010, **39**, 1203–1217.

15 K. Kang, S. S. Lee, K. Hyun, S. J. Lee and J. M. Kim, *Nat Comm*, 2013, **4**, year.

16 B. Ho and L. Leal, *J Fluid Mech*, 1976, **76**, 783–799.

17 L. G. Leal, *J Non-Newtonian Fluid Mech*, 1979, **5**, 33–78.

18 G. D'Avino, G. Romeo, M. M. Villone, F. Greco, P. A. Netti and P. L. Maffettone, *Lab Chip*, 2012, **12**, 1638–1645.

19 G. Romeo, G. D'Avino, F. Greco, P. A. Netti and P. L. Maffettone, *Lab Chip*, 2013, **13**, 2802–2807.

20 M. Villone, G. D'Avino, M. Hulsen, F. Greco and P. Maffettone, *J Non-Newtonian Fluid Mech*, 2013, **195**, 1–8.

21 K. W. Seo, H. J. Byeon, H. K. Huh and S. J. Lee, *RSC Adv*, 2014, **4**, 3512–3520.

22 C. Macosko, *Rheology: Principles, measurements, and applications. 1994*.

23 X. Xuan, J. Zhu and C. Church, *Microfluid Nanofluid*, 2010, **9**, 1–16.

24 J. Zilz, C. Schäfer, C. Wagner, R. J. Poole, M. A. Alves and A. Lindner, *Lab Chip*, 2014, **14**, 351–358.

25 E. J. Lim, T. J. Ober, J. F. Edd, S. P. Desai, D. Neal, K. W. Bong, P. S. Doyle, G. H. McKinley and M. Toner, *Nat Comm*, 2014, **5**, year.

26 R. G. Larson, *The structure and rheology of complex fluids*, Oxford university press New York, 1999, vol. 4.

27 A. Lindner, J. Vermant and D. Bonn, *Phys A*, 2003, **319**, 125–133.

28 A. Zell, S. Gier, S. Rafai and C. Wagner, *J Non-Newtonian Fluid Mech*, 2010, **165**, 1265–1274.

29 V. Tirtaatmadja, G. H. McKinley and J. J. Cooper-White, *Phys Fluids*, 2006, **18**, 043101.

30 J. Meissner and J. Hostettler, *Rheol Acta*, 1994, **33**, 1–21.

31 J. A. Pathak and S. D. Hudson, *Macromolecules*, 2006, **39**, 8782–8792.

32 C. J. Pipe and G. H. McKinley, *Mech Res Comm*, 2009, **36**, 110–120.

33 N.-T. Nguyen, Y.-F. Yap and A. Sumargo, *Meas Sci Tech-*

nol, 2008, **19**, 085405.
34 A. Groisman and V. Steinberg, *Nature*, 2001, **410**, 905–908.
35 M. Rubinstein and R. Colby, *Polymers Physics*, Oxford, 2003.
36 R. H. Colby, *Rheol Acta*, 2010, **49**, 425–442.
37 G. Segré and A. Silberberg, *Nature*, 1961, **189**, year.
38 H. Stone, *J Fluid Mech*, 2000, **409**, 165–183.
39 K. Ishii and H. Hasimoto, *J Phys Soc Japan*, 1980, **48**, 2144–2155.
40 C. E. Brennen, *Fundamentals of multiphase flow*, Cambridge University Press, 2005.
41 M. Doi and S. Edwards, *The theory of polymer dynamics*, Oxford University press, 1988.
42 E. Immergut and W. McDowell, *Polymer handbook*, Wiley, 1975.
43 J. Cooper-White, J. Fagan, V. Tirtaatmadja, D. Lester and D. Boger, *J Non-Newtonian Fluid Mech*, 2002, **106**, 29–59.
44 J. Ferguson, N. Hudson and B. Warren, *J Non-Newtonian Fluid Mech*, 1992, **44**, 37–54.
45 M. Tassieri, T. Waigh, J. Trinick, A. Aggeli and R. Evans, *J Rheol*, 2010, **54**, 117–131.
46 A. Pommella, V. Preziosi, S. Caserta, J. M. Cooper, S. Guido and M. Tassieri, *Langmuir*, 2013, **29**, 9224–9230.
47 N. Sastry, P. Dave and M. Valand, *Eur Polym J*, 1999, **35**, 517–525.
48 C. Bruce and W. Schwarz, *J Polym Sci Part A-2: Polym Phys*, 1969, **7**, 909–927.
49 D. Dupuis, F. Lewandowski, P. Steiert and C. Wolff, *J Non-Newtonian Fluid Mech*, 1994, **54**, 11–32.
50 J. Francois, D. Sarazin, T. Schwartz and G. Weill, *Polymer*, 1979, **20**, 969–975.
51 W. W. Graessley, *Synthesis and Degradation Rheology and Extrusion*, Springer, 1982, pp. 67–117.